ACS APPLIED MATERIALS & INTERFACES

Research Article

www.acsami.org

Electrospun Carbon Nanofibers with in Situ Encapsulated Co_3O_4 Nanoparticles as Electrodes for High-Performance Supercapacitors

Sara Abouali, Mohammad Akbari Garakani, Biao Zhang, Zheng-Long Xu, Elham Kamali Heidari, Jian-qiu Huang, Jiaqiang Huang, and Jang-Kyo Kim*

Department of Mechanical and Aerospace Engineering, The Hong Kong University of Science and Technology, Clear Water Bay, Kowloon, Hong Kong

Supporting Information

ABSTRACT: A facile electrospinning method with subsequent heat treatments is employed to prepare carbon nanofibers (CNFs) containing uniformly dispersed Co_3O_4 nanoparticles as electrodes for supercapacitors. The Co_3O_4/CNF electrodes with ~68 wt % active particles deliver a remarkable capacitance of 586 F g^{-1} at a current density of 1 A g^{-1}. When the current density is increased to 50 A g^{-1}, ~66% of the original capacitance is retained. The electrodes also present excellent cyclic stability of 74% capacity retention after 2000 cycles at 2 A g^{-1}. These superior electrochemical properties are attributed to the uniform dispersion of active particles in the CNF matrix, which functions as a conductive support. The onionlike graphitic layers formed around the Co_3O_4 nanoparticles not only improve the electrical conductivity of the electrode but also prevent the separation of the nanoparticles from the carbon matrix.

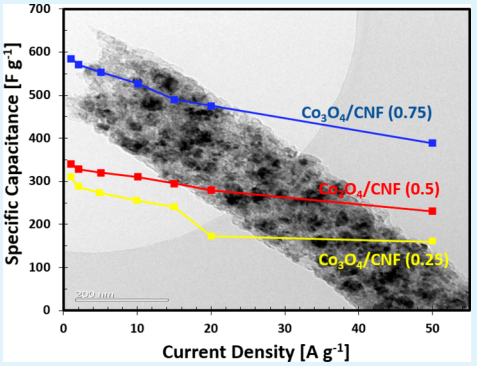

KEYWORDS: *cobalt oxide, electrospinning, carbon nanofiber, graphitization, pseudocapacitance, supercapacitor*

1. INTRODUCTION

Electrochemical supercapacitors possess power densities much higher than Li rechargeable batteries and energy densities higher than conventional capacitors, and thus can bridge the gap between the two. The energy storage mechanisms in electrochemical capacitors are usually Faradaic and non-Faradaic in nature. The Faradaic capacitance or pseudocapacitance arises from the reversible redox reactions, intercalation, or electrosorption occurring within the electroactive materials.[1−4] These supercapacitors usually consist of metal oxides and metal hydroxides such as RuO_2,[5] MnO_2,[6] NiO,[7] MoO_3,[8,9] $Co(OH)_2$,[10,11] $Ni(OH)_2$,[12] and Ni−Al double hydroxides[13] or conducting polymers such as polyaniline,[14] polypyrrole,[15] and polythiophene.[16,17] In contrast, the non-Faradaic capacitance arises from charge separation in a Helmholtz double layer at the conductive electrode/electrolyte interface. The electric double-layer capacitors (EDLCs) are mainly based on carbon materials or derivatives, such as carbon nanotubes, graphene, and activated carbon, with large surface areas.[1,18−21] With the same surface area of the electrode, the Faradaic pseudocapacitors have higher energy densities, while the EDLCs have higher power densities.[1,2]

The development of promising electrode materials is essential to optimizing the overall electrochemical performance of supercapacitors. Among different pseudocapacitive materials, RuO_2 has been extensively studied because of its simple and scalable synthesis, a wide potential window, reversible redox reactions, high theoretical specific capacitances, and high electrical conductivities. However, the toxicity and high cost limit its large scale use in supercapacitors.[22−24] Therefore, significant efforts have been directed toward finding alternative materials that are cost-effective and possess excellent performance. Cobalt spinel oxide, Co_3O_4, is found to exhibit attractive pseudocapacitive behavior due to its high theoretical specific capacitance up to 3560 F g^{-1}, excellent capacity retention, and high redox reactivity, so as to replace the state-of-the-art RuO_2.[25,26] However, Co_3O_4, similar to other transition metal oxides, suffers from a poor electrical conductivity and limited electrochemical stability during cycles. To overcome the aforementioned deficiencies, the nanostructured Co_3O_4 particles are assembled together with a carbon matrix to form composites in various forms. Coupling the unique advantages of these nanoscale dissimilar capacitive materials is a promising approach to control, develop, and optimize the structures and properties of electrode materials with enhanced performance of supercapacitors.[27] Different hybrid electrodes have thus far been made from Co_3O_4 and different carbon materials, such as Co_3O_4/graphene[28,29] and Co_3O_4/carbon nanotube (CNT),[30] with improved electrical conductivities of the electrodes and large surface contact between the active material and electrolyte for efficient chemical reactions.

However, designing a facile one-step method to produce Co_3O_4/carbon electrodes with excellent cyclic and rate performances has not been realized. Apart from graphene and

Received: March 31, 2015
Accepted: June 1, 2015
Published: June 1, 2015

DOI: 10.1021/acsami.5b02787
ACS Appl. Mater. Interfaces 2015, 7, 13503−13511

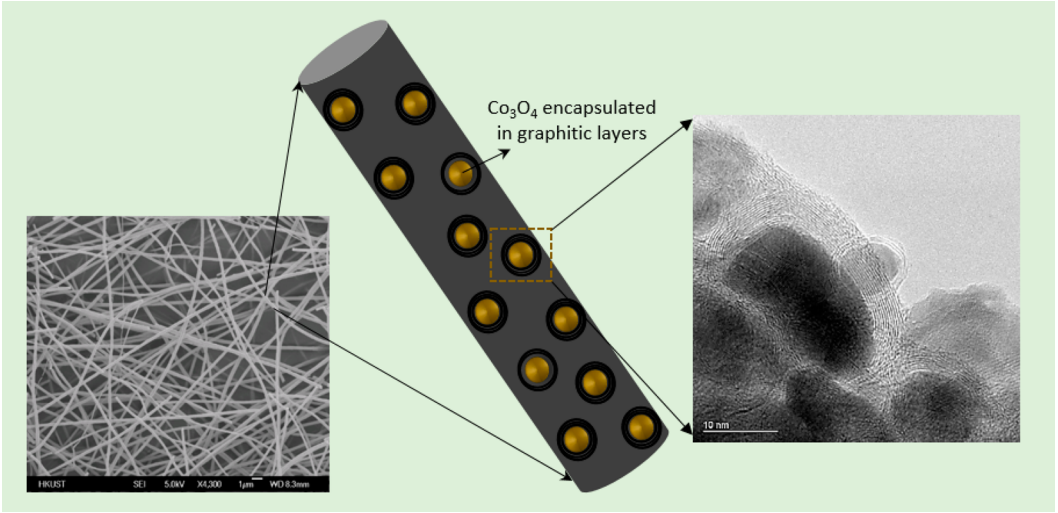

Figure 1. Schematic illustration, SEM and TEM images of Co_3O_4/CNF nanocomposite.

CNTs, electrospun carbon nanofibers (CNFs) have been widely applied as electrodes for other types of energy storage devices owing to many advantages, including their facile and environmentally benign process and high conductivities as well as functioning as stress buffer to accommodate the volumetric strains of active particles.[31−33] Another advantage of using CNFs as the substrate for active materials is that the electric double-layer capacitance and pseudocapacitance function simultaneously, depending on the nature of the electrode material.[34,35] Herein, we present a facile synthesis of CNFs containing Co_3O_4 nanoparticles with surrounding graphitic layers for applications in high-performance supercapacitors.

2. EXPERIMENTAL SECTION

2.1. Materials and Synthesis of Co_3O_4/carbon nanofiber. Polyacrilonitrile (PAN, average Mw = 150 000 supplied by Aldrich) was used as the precursor, and *N*,*N*-dimethylformamide (DMF) was used as the solvent to prepare the carbon nanofiber (CNF) matrix solution. Cobalt(II) acetate tetrahydrate (CoAc, supplied by UNI-CHEM) was used as the source of Co.[36] In a typical process, 0.6 g of PAN and 0.45 g of CoAc were dissolved in 10 mL of DMF at 80 °C for 5 h under magnetic stirring. The mixture was transferred to a plastic capillary and electrospun on a spinning machine (KATO Tech. Co.) at 16 kV. The collector-to-needle distance was maintained at 15 cm to collect a light-pink film on an aluminum foil wrapped around a drum collector rotating at a speed of 0.6 m min^{-1}. The film was stabilized at 250 °C for 90 min in air and carbonized at 650 °C for 1 h in a nitrogen atmosphere of a tube furnace. The carbonized films were post-heat treated at 300 °C for 15 min in air to precipitate Co_3O_4 nanoparticles. In an effort to identify an optimized composition, different amounts of CoAc were added into the fixed amount of polymer precursor, namely, 0.15, 0.3, and 0.45 g, for 0.6 g of polymer. On the basis of the mass ratio of CoAc to PAN, the final products were labeled as Co_3O_4/CNF (0.25), Co_3O_4/CNF (0.5), and Co_3O_4/CNF (0.75). Higher amounts of CoAs resulted in difficulties in electrospinning and brittle CNF films after post-heat treatment; thus, no further attempts were made to increase the CoAc content. For comparison, neat CNFs were also prepared using the same procedure without adding CoAc. Figure 1 schematically shows the microstructure of the prepared composite CNFs.

2.2. Structural Characterization. The microstructures and morphologies of the materials were studied on a scanning electron microscope (SEM, JEOL 6300) and a field emission transmission electron microscope (FETEM, JEOL 2010F). The crystal structure was evaluated on a powder X-ray diffraction (XRD) system (PW1830, Philips) with Cu Kα radiation. The X-ray photoelectron spectroscopy (XPS, Surface analysis PHI5600, Physical Electronics) was employed to evaluate the surface chemistry of the materials, using a monochromatic Al Kα X-ray at 14 kV. Thermogravimetric analysis (TGA) was conducted (TGA/DTA 92 Setaram II testing system) in air over a temperature range of 50−800 °C at a heating rate of 10 °C min^{-1}. Nitrogen absorption/desorption isotherms were obtained on a Micromeritics ASAP 2020 analyzer at 77 K and the corresponding surface areas were determined using the Brunauer−Emmett−Teller (BET) method. The sheet resistance of Co_3O_4/CNF films with different Co_3O_4 contents was measured based on the four-point probe method (Scientific Equipment & Services) using the films on a glass slide.

2.3. Electrochemical Measurements. All electrochemical measurements were performed in a beaker-type three-electrode system in 6 M KOH aqueous electrolyte at room temperature. A platinum plate and a saturated Ag/AgCl electrode were used as the counter electrode and reference electrode, respectively. The working electrode was prepared by mixing Co_3O_4/CNFs with conductive carbon black (super P) and polyvinylidene fluoride (PVDF) as the binder dissolved in *N*-methyl-2-pyrrolidone (NMP) in the weight ratio of 70:10:20. Then, the resulting mixture was coated onto the Ni foam substrate of 10 mm × 10 mm square, which was used as the current collector. The foam was dried at 80 °C for 12 h in air to evaporate the solvent. The prepared electrodes were tested using a cyclic voltammetry (CV) method and galvanostatic charge/discharge chronopotentiometry (CP) on an electrochemical workstation (CHI 660C). These measurements were made at a potential window of −0.05−0.45 V at different scanning rates from 10 to 100 mV s^{-1} and current densities from 1 to 50 A g^{-1}. The specific capacitance (C_s) was calculated using the galvanostatic charge/discharge data according to eq 1:

$$C_s = \frac{It}{m\Delta V} \tag{1}$$

where I is the applied current, m is the mass of the active material, ΔV is the potential range, and t is the time for discharge.

To have a better evaluation of the electrochemical performance, the two-electrode configuration cell was also assembled using the optimized materials. Two pieces of identical electrodes were separated by a filter paper as the separator, which was soaked in KOH 6 M for 12 h before the assembly of the symmetric cell. The measurements were performed at a potential window from 0 to 1 V, and the specific capacitance C_s was calculated using the following equation:

$$C_s = \frac{4It}{m\Delta V} \tag{2}$$

DOI: 10.1021/acsami.5b02787
ACS Appl. Mater. Interfaces 2015, 7, 13503−13511

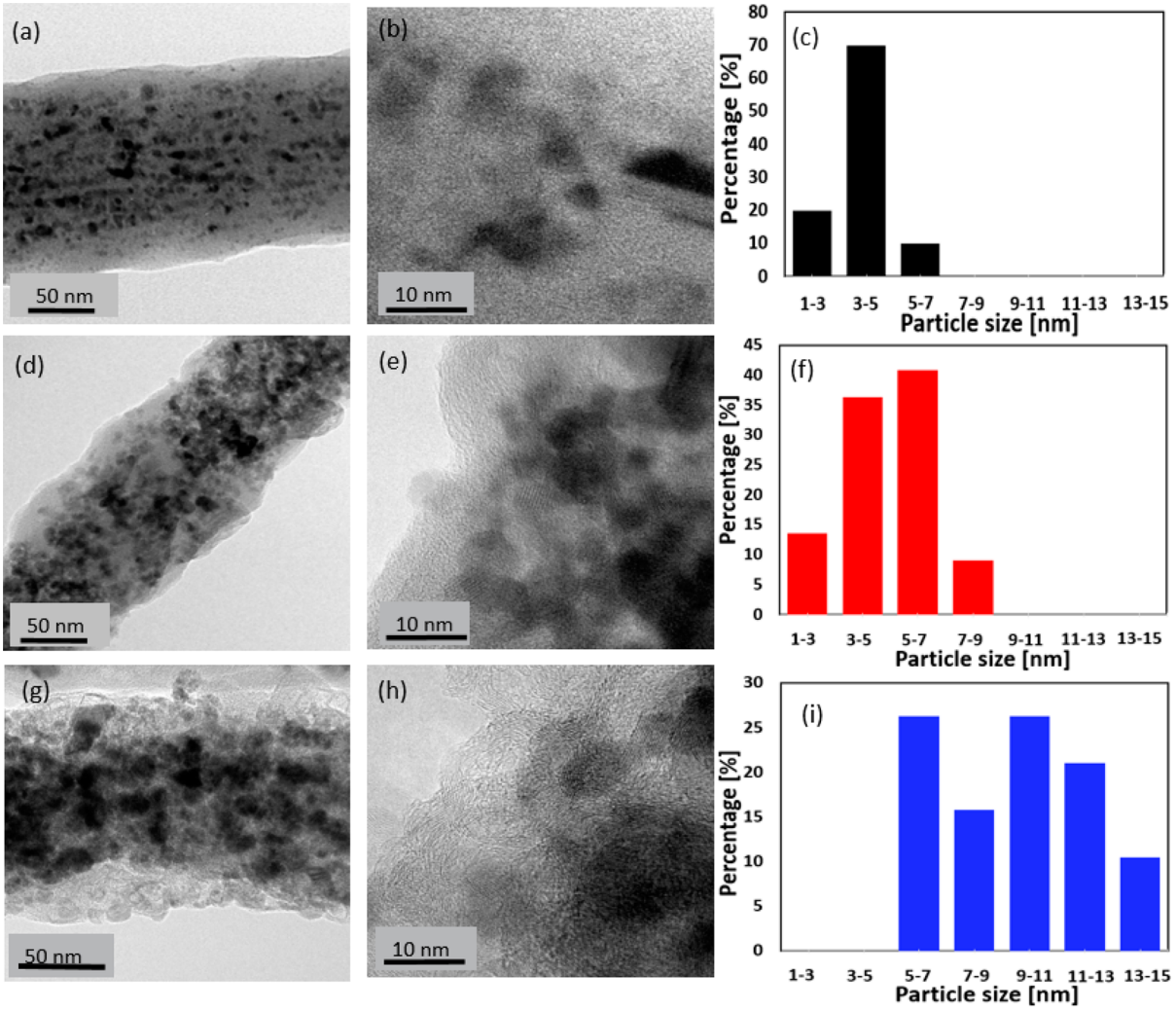

Figure 2. TEM images and particle size distributions of Co_3O_4/CNFs prepared using different CoAc contents: (a, b, c) 0.25, (d, e, f) 0.5, and (g, h, i) 0.75.

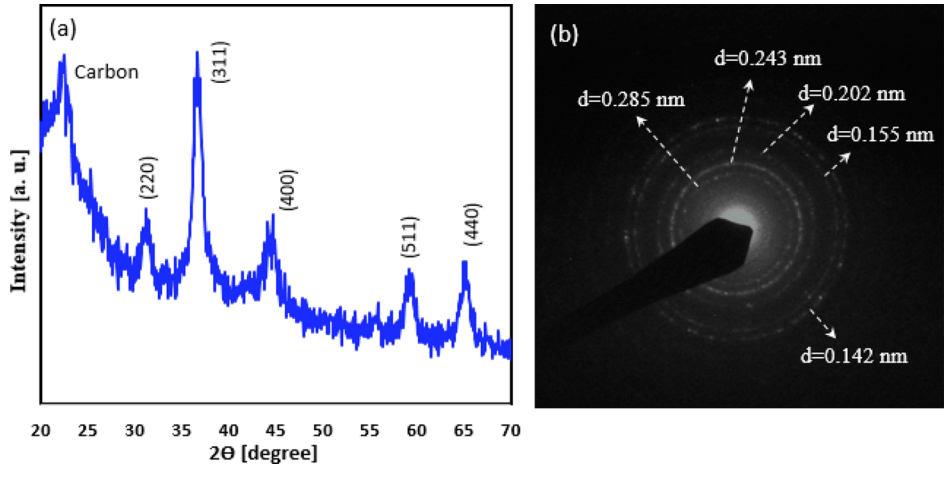

Figure 3. (a) XRD and (b) SAED patterns of Co_3O_4/CNF (0.75).

3. RESULTS AND DISCUSSION

3.1. Material Characteristics of Co_3O_4/CNF Composites. The SEM image of the electrospun Co_3O_4/CNFs with a CoAc to PAN ratio of 0.75 is shown in Figure 1, while the SEM images and the diameter distribution charts of the other composites are presented in Supporting Information, Figure S1. All materials with different CoAc contents showed similar, uniform bead-free nanofibers with diameters mostly in the range of 150−300 nm. The fiber diameters tended to become marginally smaller when the ratio of CoAc increased in the

DOI: 10.1021/acsami.5b02787
ACS Appl. Mater. Interfaces 2015, 7, 13503−13511

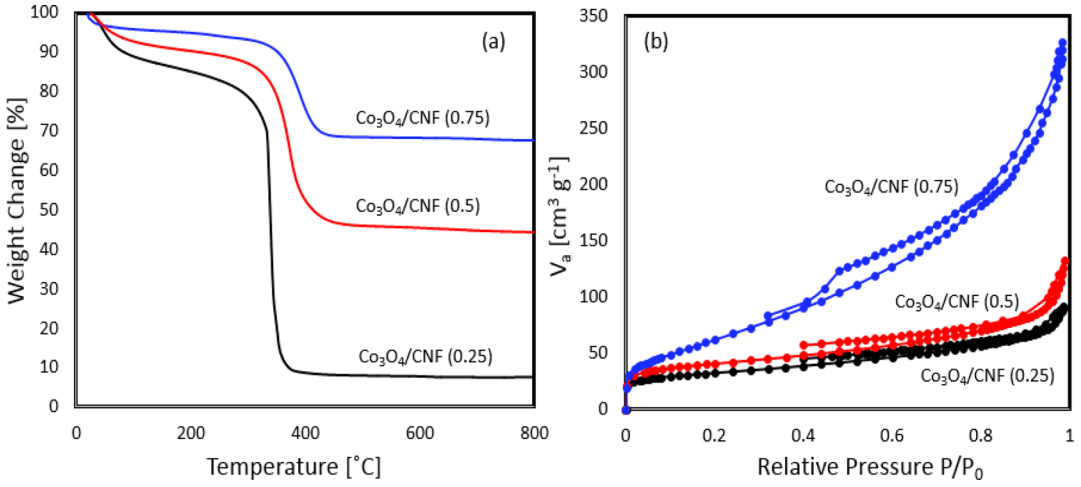

Figure 4. (a) TGA curves and (b) nitrogen absorption/desorption isotherms for Co_3O_4/CNF composites prepared using different CoAc contents.

Table 1. Atomic Concentrations of the Elements, Electrical Conductivities, Surface Areas, sp^2/sp^3 Intensity Ratios, and I_D/I_G Ratios of Co_3O_4/CNF Nanocomposites Containing Different Amounts of CoAc Precursor

	compositions [atom %]							
samples	C	N	O	Co	conductivity [S cm^{-1}]	surface area [m^2 g^{-1}]	sp^2/sp^3 intensity ratio	I_D/I_G ratio
Co_3O_4/CNF (0.25)	80.5	11.1	6.2	2.2	1.4×10^{-4}	113.8	1.21	1.36
Co_3O_4/CNF (0.5)	79.0	11.2	7.3	2.6	3.8×10^{-5}	143.2	1.39	1.27
Co_3O_4/CNF (0.75)	75.9	2.4	13.3	8.4	4.0×10^{-3}	230.6	3.05	0.97

solution as a result of the lower carbon content in the composite. It is worth noting that after postannealing in air the nanofibers maintained their fibrous structure, partly confirming proper heat treatment conditions used in this study. The TEM images of the CNFs are presented in Figure 2. The number of nanoparticles embedded in the CNFs increased with the increasing ratio of CoAc/PAN from 0.25 to 0.75. Further, the particle size distribution charts (Figure 2c,f,i) confirm that the diameters of the nanoparticles varied very similarly to the CoAc content. These observations signify that with increasing the mass ratio of CoAc/PAN, the nanoparticles tended to aggregate and form larger particles, while their numbers also increased.

Figure 3 shows the XRD pattern as well as the SAED pattern for Co_3O_4/CNF (0.75), both confirming that the spherical nanoparticles were Co_3O_4 crystals. The major peaks (Figure 3a) were located at 31.2, 36.8, 44.8, 59.3, and 65.2° corresponding to the (220), (311), (400), (511), and (440) reflections of Co_3O_4 (JCPDS No. 078−1970). The ring patterns (Figure 3b) indicate the lattice *d*-spacings of 2.85, 2.43, 2.02, 1.55, and 1.42 Å related to the (220), (311), (400), (511), and (440) planes of cubic Co_3O_4 and are in agreement with the results of XRD. To quantify the compositions of the three composites, TGA was performed in air, and the curves are shown in Figure 4a. All samples presented essentially similar weight change behaviors: an initial weight loss started to occur below 220 °C, followed by a sharp weight loss at ∼310−370 °C due to burning of carbon. The abrupt weight loss at this temperature range varied inversely to the CoAc precursor content. Starting from ∼400 and to 800 °C, all samples exhibited a steady-state constant value with the remaining Co_3O_4 weight ∼8, 46, and 68 wt % in Co_3O_4/CNF (0.25), Co_3O_4/CNF (0.5), and Co_3O_4/CNF (0.75), respectively. The nitrogen absorption/desorption isotherms are shown in Figure 4b, and the BET specific surface areas of the composites are summarized in Table 1, showing the increase in surface area by increasing the cobalt precursor, consistent with the TEM images of the nanofibers in Figure 2. Also note that the surface of the CNFs became rougher with a higher CoAc content as a result of CoAc decomposition during the heat treatments, while the gaseous products emerged from the fibers, creating pores and a rough surface.[37]

To investigate the bonding state and chemical elements, the XPS analysis was performed for the Co_3O_4/CNF (0.75) composite, and the results are shown in Figure 5. The other Co_3O_4/CNF composites prepared from different Co precursor contents presented essentially similar XPS spectra with different elemental compositions, as shown in Table 1. The deconvoluted C 1s spectrum (Figure 5b) showed four binding

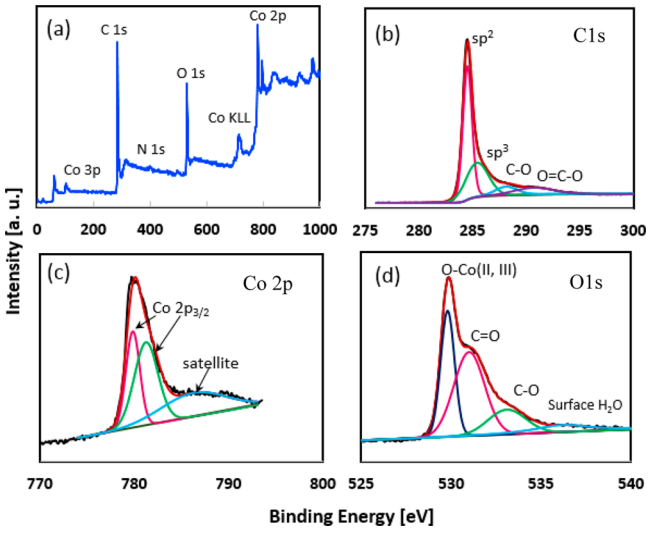

Figure 5. (a) General XPS spectrum and deconvoluted XPS spectra of (b) C 1s, (c) Co 2p, and (d) O 1s for Co_3O_4/CNF (0.75).

DOI: 10.1021/acsami.5b02787
ACS Appl. Mater. Interfaces 2015, 7, 13503−13511

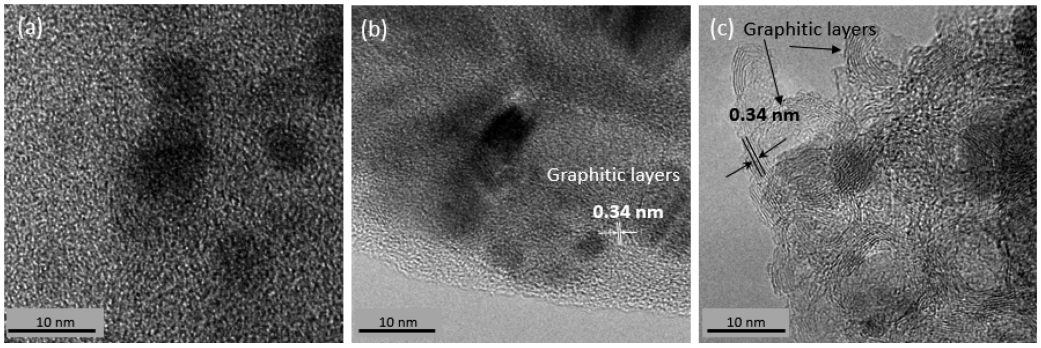

Figure 6. HRTEM image of (a) Co_3O_4/CNF (0.25), (b) Co_3O_4/CNF (0.5), and (c) Co_3O_4/CNF (0.75).

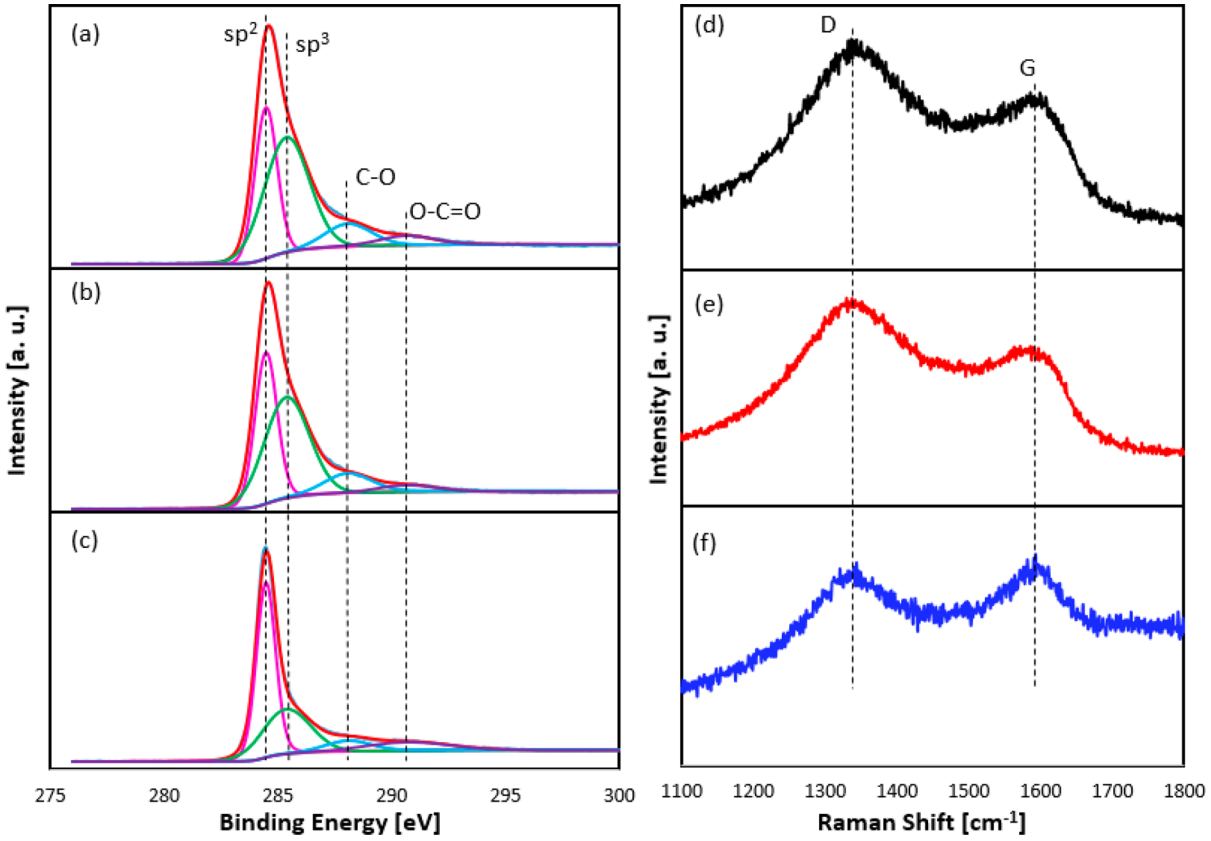

Figure 7. XPS deconvoluted C 1s spectra and Raman spectra of (a, d) Co_3O_4/CNF (0.25), (b, e) Co_3O_4/CNF (0.5), and (c, f) Co_3O_4/CNF (0.75).

energies at 284.5, 285.4, 288.1, and 290.7 eV, corresponding to sp^2 and sp^3 hybridized carbon, C−O and O═C−O functional groups, respectively.[38] Figure 5c exhibited two main peaks at 779.8 and 781.4 eV corresponding to Co $2p_{3/2}$ and a satellite at 786.2 eV, in agreement with the previous reports for Co_3O_4.[39,40] The O 1s spectrum (Figure 5d) showed four peaks at 529.8, 531.3, 533.2, and 536.2 eV attributed, respectively, to the oxygen species in cobalt spinel oxide, oxygen bonds in C═O, C−O, and adsorbed surface water.[40−42] The elemental compositions shown in Table 1 confirm the TGA results (Figure 4a) where the large difference between the carbon and Co_3O_4 contents obtained from these two analytical methods can be attributed to the very low penetration depth of X-ray photoelectrons.

The electrical conductivities of the composites are shown in Table 1. It is of interest to note that the Co_3O_4/CNF (0.75) composite containing the largest amount of Co_3O_4 had the highest electrical conductivity, which is 1 to 2 orders of magnitude higher than those with lower contents of Co_3O_4 or neat CNFs (4×10^{-5} S cm^{-1}). The as-prepared CNF networks largely remained in the form of porous fiber web on the sub-micrometer scale even after preparing the electrode by mixing with carbon black and PVDF additives. Thus, it can be said that the electrical conductivities of the neat materials represent those of the slurry-coated. To have a better understanding, more high-resolution (HR) TEM images were taken from all samples, as shown in Figure 6. Clearly, there was a network of graphitic layers created in Co_3O_4/CNF (0.75) (Figure 6c), which may be responsible for the largely enhanced electrical conductivity, whereas the graphitic layers were hardly formed in both Co_3O_4/CNF (0.25) and Co_3O_4/CNF (0.50) (Figure 6a,b). The HRTEM images of the neat CNFs presented in Supporting Information, Figure S2 indicate an almost completely amorphous structure of CNFs. During the carbon-

DOI: 10.1021/acsami.5b02787
ACS Appl. Mater. Interfaces 2015, 7, 13503−13511

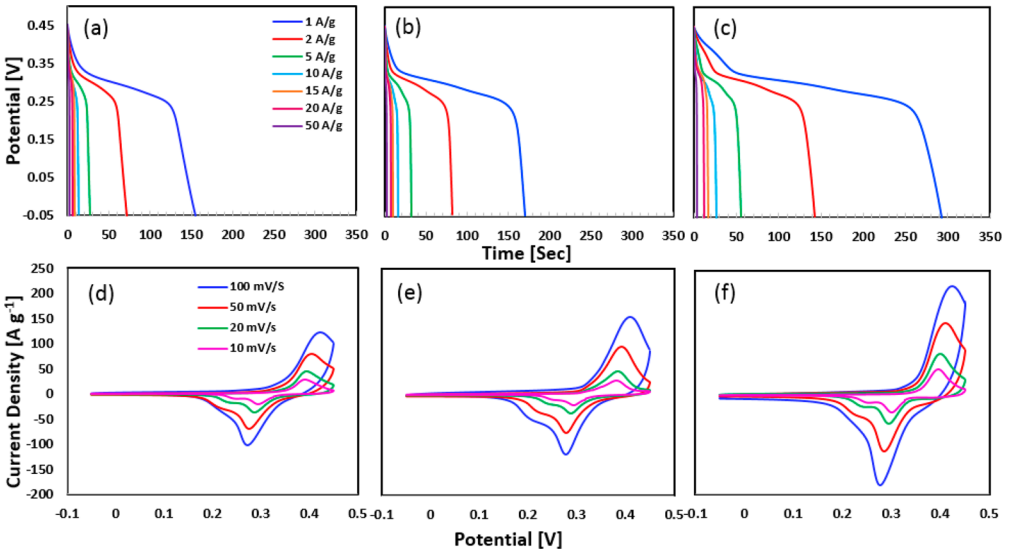

Figure 8. Discharge profiles of (a) Co_3O_4/CNF (0.25), (b) Co_3O_4/CNF (0.5), and (c) Co_3O_4/CNF (0.75) electrodes at different current densities. CV curves of (d) Co_3O_4/CNF (0.25), (e) Co_3O_4/CNF (0.5), and (f) Co_3O_4/CNF (0.75) electrodes at different scan rates.

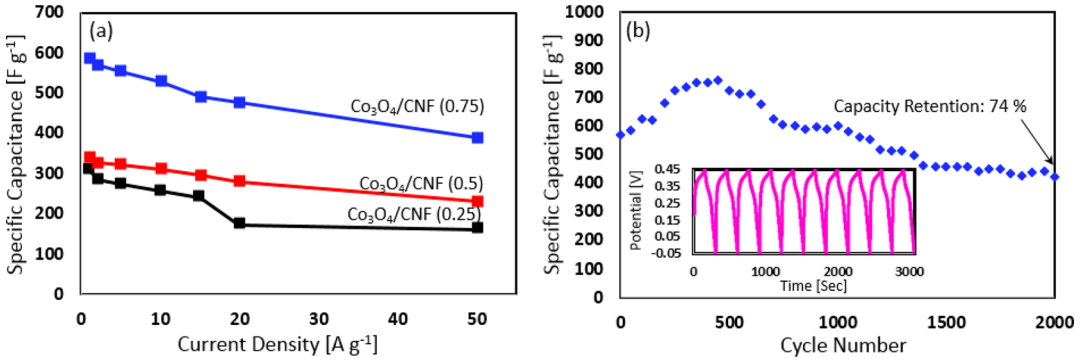

Figure 9. (a) Specific capacitance vs current density for different electrode materials and (b) cyclic performance of Co_3O_4/CNF (0.75) at 2 A g^{-1}. (inset) Charge/discharge profiles for the first 10 cycles.

ization process, the cobalt precursor was reduce to metallic cobalt, which acted as a catalyst to crystallize the surrounded amorphous carbon to form graphitic layers.[43,44] The graphitization around the metal nanoparticles taking place during the heat treatment involved the dissolution of amorphous carbon into catalyst particles, followed by the precipitation of graphitic carbon.[44−47] The graphitic layers have other advantages, such as complete encapsulation of nanoparticles within the CNFs (Figures 1 and 6), thus preventing them from separation from the CNF substrate.[44,47] The large particle size may have also played a positive role in the graphitization process by stimulating the dissolution and precipitation of carbon around the Co_3O_4 particles. It is unclear, however, as to why the electrical conductivities of the composites did not vary exactly with the Co precursor content. It could be attributed to the balance between the ratio of conductive carbon substrate to low conductivity Co_3O_4 phase and the degree of graphitization. Also note that the continuous graphene networks could also function as protective shell to prevent the separation of nanoparticles from the CNFs during the charge/discharge processes.[36,48]

To quantify the degree of graphitization, C 1s XPS spectra of the three composites were further studied and compared in Figure 7. The intensity ratio of sp^2 to sp^3 binding energies of C 1s spectrum is known to be a good measure of the degree of graphitization.[49−53] Here, the sp^2 to sp^3 ratios for the Co_3O_4/CNF (0.25), Co_3O_4/CNF (0.5), and Co_3O_4/CNF (0.75) composites changed from 1.21 to 1.39 and 3.05, respectively. This implies that the highest degree of graphitization occurred in the composite with the highest Co_3O_4 content and the largest size of Co_3O_4 nanoparticles in agreement with the HRTEM observations. Besides, the line shape of the XPS C 1s spectrum also provides an indication of the degree of graphitization on a carbon fiber surface where a narrower and a more asymmetric C ls spectrum corresponds to a more complete graphite lattice structure.[54] The narrowest and least asymmetric shape of Co_3O_4/CNF (0.75) among the three composites further confirmed the above conclusion.

The Raman spectroscopy was also employed to investigate the degree of graphitization, and the results are shown in Figure 7d−f and Supporting Information, Figure S2c. The I_D/I_G intensity ratio is a good measure of the degree of graphitization since the higher ratio of I_D/I_G corresponds to a lower degree of graphitization in carbon materials.[55] Here, the I_D/I_G ratio (Table 1) changed from 1.41 for the neat CNFs to 1.36, 1.27, and 0.97 for the Co_3O_4/CNF (0.25), Co_3O_4/CNF (0.5), and Co_3O_4/CNF (0.75) composites, respectively, which is consistent with the previous results.

3.2. Electrochemical Properties of Co_3O_4/CNF Composite Electrodes. The Co_3O_4/CNF composites were used as

DOI: 10.1021/acsami.5b02787
ACS Appl. Mater. Interfaces 2015, 7, 13503−13511

the electrodes for supercapacitors, and their electrochemical performances were evaluated using a three-electrode cell, and the results are shown in Figure 8. A plateau was observed in the discharge curves of all electrode materials especially at low current densities (Figure 8a–c), a typical of pseudocapacitive characteristics.[56] Figure 8d–f presents typical cyclic voltammetry (CV) curves of the electrodes at various scan rates between 10 and 100 mV s^{-1}. At a low scan rate of 10 mVs^{-1}, two current peaks were identified at ~0.25 and ~0.3 V during the cathodic sweep, and the corresponding Faradaic reactions are described by

$$Co_3O_4 + OH^- + H_2O \leftrightarrow 3CoOOH + e^- \quad (3)$$

$$CoOOH + OH^- \leftrightarrow CoO_2 + H_2O + e^- \quad (4)$$

When the scan rate was changed from 10 to 100 mV s^{-1}, the shape of the CV curves remained much the same showing the excellent electrochemical reversibility of the electrodes. On the basis of the discharging time obtained from the CP curves in Figure 8a–c and using eq 1, the specific capacitances were calculated and are plotted in Figure 9a as a function of current density. The composite electrode with the highest Co_3O_4 content, Co_3O_4/CNF (0.75), delivered a specific capacitance of 586 F g^{-1} at 1 A g^{-1} the highest among the three electrodes. With increasing current density from 1 to 2, 5, 10, 15, 20, and 50 A g^{-1} the specific capacitances were gradually reduced to 570, 554, 528, 490, 476, and 389 F g^{-1}, respectively. This observation is equivalent to excellent capacitance retention of 66% when the current density was increased from 1 to 50 A g^{-1}. The corresponding specific capacitances were 341 and 310 F g^{-1} for the Co_3O_4/CNF (0.5) and Co_3O_4/CNF (0.25) electrodes at 1 A g^{-1} and presented much the similar trends with 50–60% lower capacitances than those of the Co_3O_4/CNF (0.75) electrode, when the current density was increased. It should be mentioned that because the electrochemical activity of the neat CNFs was negligible, that is, only 6 F g^{-1} in 1 A g^{-1}, see Supporting Information, Figure S3, in KOH electrolyte in the same voltage window,[56] the capacitance of the Co_3O_4/CNFs nanocomposite electrodes arose mainly from Co_3O_4 nanoparticles.

Figure 9b shows the cycling performance of the Co_3O_4/CNF (0.75) electrode at a current density of 2 A g^{-1}, and the inset in Figure 9b presents the corresponding charge/discharge profiles, confirming the stable electrochemical behavior of the electrode. The specific capacitance gradually increased from 570 F g^{-1} and reached a maximum of 760 F g^{-1} at ~450th cycle, more than 133% of the initial capacitance in the first cycle. This interesting observation is attributed to very slow activation of the Co_3O_4 nanoparticles during the first 450 cycles. Only a fraction of the electrode material was active during the initial few hundred cycles, while the other part was not activated. As the electrolyte gradually penetrated into the CNFs, more nanoparticles were activated and contributed to the capacitance of the electrode.[57] The peak was followed by a gradual decrease before reaching 424 F g^{-1} after 2000 cycles. The gradual decay of capacitance is typical of pseudocapacitive electrodes with such a high loading of metal oxide.[34,58,59] The capacitance showed a stable behavior in the final 700 cycles with a capacitance retention of ~74%. Major reasons behind the excellent specific capacitances and capacitance retention at high current densities are due to full encapsulation of the uniformly dispersed Co_3O_4 nanoparticles within the CNF matrix, which prevented the particles from detachment during cycles, and the presence of conducting networks offered by the carbon matrix with an enhanced electrical conductivity. The uniformly dispersed nanoparticles increased the surface area of the active material that was in contact with the electrolyte and actively participated in redox reaction. The increase in Co_3O_4 content from 0.25 to 0.75 meant an enhanced surface roughness and surface area of the nanofibers, as well as a much higher electrical conductivity ameliorated by the interconnected graphitic layers along the fiber, resulting in better cyclic stability and high rate performance.

The optimized electrode Co_3O_4/CNF (0.75) was further tested in a symmetric cell, and the discharge profiles as well as the CV curves are presented in Supporting Information, Figure S4. According to the discharge profiles (Figure S4b) and eq 2, the device delivered specific capacitances of 299.2, 234.4, 172, and 120.6 F g^{-1} when the current density was changed from 1 to 2, 5, and 10 A g^{-1}.

The supercapacitive performance of the electrodes developed in this study was compared to those of similar carbon-based electrodes containing Co_3O_4 particles, as shown in Table 2,

Table 2. Comparison of Specific Capacitances between the Current Study and Similar Electrodes Reported in the Literature

material	preparation method	specific capacitance [F g^{-1}]	current density [A g^{-1}]	ref
porous Co_3O_4 film	electrodeposition	443	2	25
CNF/$Co(OH)_2$	electrospinning +treatment	135	2	34
Co_3O_4/graphene	hydrothermal	60	2	58
Co_3O_4/CNF	electrospinning	524	2	56
Co_3O_4 film	plasma spraying	150	2.75	59
Co_3O_4/rGO	hydrothermal	416	2	29
Co_3O_4/graphene	hydrothermal	420	2	28
Co_3O_4/PCNF	electrospinning	570	2	current study

where the preparation methods are also included. Clearly, theCo_3O_4/CNF (0.75) electrode presented the highest specific capacitance at a given current density of 2 A g^{-1} among all similar electrode materials ever reported in the literature. Besides, the facile electrospinning method used to in situ encapsulate fine Co_3O_4 nanoparticles within the porous CNFs is considered a great advantage over the other preparation methods.

4. CONCLUSION

A facile electrospinning method was used to encapsulate cobalt oxide nanoparticles within continuous carbon nanofibers. The cobalt precursor to PAN weight ratio was varied to identify an optimal Co_3O_4 nanoparticle content in the final electrospun CNFs. They were used as the working electrodes in three-electrode supercapacitor cells. The results showed that the Co_3O_4/CNF (0.75) electrode containing the highest cobalt oxide content presented the highest specific capacitances in all current densities ranging from 1 to 50 A g^{-1} with excellent rate performance and cyclic stability. The Co_3O_4/CNF (0.75) electrode delivered specific capacitances of 586 and 389 F g^{-1} at

DOI: 10.1021/acsami.5b02787
ACS Appl. Mater. Interfaces 2015, 7, 13503–13511

1 and 50 A g^{-1}, respectively, along with 424 F g^{-1} after 2000 cycles at a moderate current density of 2 A g^{-1}, which is equivalent to 74% capacitance retention. These superior properties are attributed to uniform dispersion of fine Co_3O_4 nanoparticles in the CNF matrix, which acted as conducting support for the active nanoparticles. Moreover, the onionlike graphitic layers formed around the Co_3O_4 nanoparticles improved the electronic conductivity while preventing the particles from detachment from the CNF. The comparison with existing data indicates that the Co_3O_4/CNF electrode exhibited the highest capacity among similar Co_3O_4-based electrode materials. In view of the low-cost and simple preparation method, the synthesized material can be a promising electrode for high-performance supercapacitors.

■ ASSOCIATED CONTENT

Supporting Information

SEM images and nanofiber diameter distributions of Co_3O_4/CNFs, TEM images and Raman spectrum of neat CNFs, discharge profiles and CV curves of neat CNFs and symmetric cell. The Supporting Information is available free of charge on the ACS Publications website at DOI: 10.1021/acsami.5b02787.

■ AUTHOR INFORMATION

Corresponding Author

*E-mail: mejkkim@ust.hk. Phone: +852 2358 7207. Fax: +852 2358 1543.

Notes

The authors declare no competing financial interest.

■ ACKNOWLEDGMENTS

This project was financially supported by the Research Grants Council of Hong Kong SAR (GRF Project Code 613612). S.A. was the recipient of a Hong Kong Ph.D. Fellowship Award. The authors also appreciate the technical assistance from the Materials Characterization and Preparation Facilities (MCPF) of HKUST.

■ REFERENCES

(1) Zhang, L. L.; Zhao, X. S. Carbon-Based Materials as Supercapacitor Electrodes. *Chem. Soc. Rev.* **2009**, *38*, 2520−2531.

(2) Zhi, M.; Xiang, C.; Li, J.; Li, M.; Wu, N. Nanostructured Carbon−Metal Oxide Composite Electrodes for Supercapacitors: A Review. *Nanoscale* **2013**, *5*, 72−88.

(3) Wang, G.; Zhang, L.; Zhang, J. A Review of Electrode Materials for Electrochemical Supercapacitors. *Chem. Soc. Rev.* **2012**, *41*, 797−828.

(4) Obreja, V. V. N. On the Performance of Supercapacitors with Electrodes Based on Carbon Nanotubes and Carbon Activated Material-A Review. *Phys. E* **2008**, *40*, 2596−2605.

(5) Hu, C. C.; Chang, K. H.; Lin, M. C.; Wu, Y. T. Design and Tailoring of the Nanotubular Arrayed Architecture of Hydrous RuO_2 for Next Generation Supercapacitors. *Nano Lett.* **2006**, *6* (12), 2690−2695.

(6) Lin, Y. H.; Wei, T. Y.; Chien, H. C.; Lu, S. Y. Manganese Oxide/Carbon Aerogel Composite: An Outstanding Supercapacitor Electrode Material. *Adv. Energy Mater.* **2011**, *1*, 901−907.

(7) Yuan, C.; Zhang, X.; Su, L.; Gao, B.; Shen, L. Facile Synthesis and Self-Assembly of Hierarchical Porous NiO Nano/Micro Spherical Superstructures for High Performance Supercapacitors. *J. Mater. Chem.* **2009**, *19*, 5772−5777.

(8) Jiang, F.; Li, W.; Zou, R.; Liu, Q.; Xu, K.; An, L.; Hu, J. MoO_3/PANI Coaxial Heterostructure Nanobelts by in situ Polymerization for High Performance Supercapacitors. *Nano Energy* **2014**, *7*, 72−79.

(9) Zhao, G.; Zhang, N.; Sun, K. Porous MoO_3 Films with Ultra-Short Relaxation Time Used for Supercapacitors. *Mater. Res. Bull.* **2013**, *48*, 1328−1332.

(10) Tang, J.; Liu, D.; Zheng, Y.; Li, X.; Wang, X.; He, D. Effect of Zn-Substitution on Cycling Performance of a-$Co(OH)_2$ Nanosheet Electrode for Supercapacitors. *J. Mater. Chem. A* **2014**, *2*, 2585−2591.

(11) Tang, Y.; Liu, Y.; Yu, S.; Mu, S.; Xiao, S.; Zhao, Y.; Gao, F. Morphology Controlled Synthesis of Monodisperse Cobalt Hydroxide for Supercapacitor with High Performance and Long Cycle Life. *J. Power Sources* **2014**, *256*, 160−169.

(12) Li, Q.; Ni, H.; Cai, Y.; Cai, X.; Liu, Y.; Chen, G.; Fan, L. Z.; Wang, Y. Preparation and Supercapacitor Application of the Single Cystal Nickel Hydroxide and Oxide Nanosheets. *Mater. Res. Bull.* **2013**, *48*, 3518−3526.

(13) Memon, J.; Sun, J.; Meng, D.; Ouyang, W.; Memon, M. A.; Huang, Y.; Yan, S.; Geng, J. Synthesis of Graphene/Ni−Al Layered Double Hydroxide Nanowires and Their Application as an Electrode Material for Supercapacitors. *J. Mater. Chem. A* **2014**, *2*, 5060−5067.

(14) Huang, Z. D.; Liang, R.; Zhang, B.; He, Y. B.; Kim, J. K. Evolution of Flexible 3D Graphene Oxide/Carbon Nanotube/Polyaniline Composite Papers and Their Supercapacitive Performance. *Compos. Sci. Technol.* **2013**, *88*, 126−133.

(15) Shi, Y.; Pan, L.; Liu, B.; Wang, Y.; Cui, Y.; Bao, Z.; Yu, G. Nanostructured Conductive Polypyrrole Hydrogels as High-Performance, Flexible Supercapacitor Electrodes. *J. Mater. Chem. A* **2014**, *2*, 6086−6091.

(16) Zhang, H.; Hu, Z.; Li, M.; Hu, L.; Jiao, S. A High-Performance Supercapacitor Based on a Polythiophene/Multiwalled Carbon Nanotube Composite by Electropolymerization in an Ionic Liquid Microemulsion. *J. Mater. Chem. A* **2014**, *2*, 17024−17030.

(17) Ramya, R.; Sivasubramanian, R.; Sangaranarayanan, M. V. Conducting Polymers-Based Electrochemical Supercapacitors-Progress and Prospects. *Electrochim. Acta* **2013**, *101*, 109−129.

(18) Huang, Z. D.; Zhang, B.; Zheng, Q.; Oh, S. W.; Lin, X. Y.; Yousefi, N.; Kim, J. K. Self-Assembled Reduced Graphene Oxide/Carbon Nanotube Films as Electrodes for Supercapacitors. *J. Mater. Chem.* **2012**, *22*, 3591−3599.

(19) Huang, Z. D.; Zhang, B.; Liang, R.; Zheng, Q.; Oh, S. W.; Lin, X. Y.; Yousefi, N.; Kim, J. K. Effects of Reduction Process and Carbon Nanotube Content on Supercapacitive Performance of Flexible Graphene Oxide Papers. *Carbon* **2012**, *50*, 4239−4251.

(20) Ouyang, W.; Sun, J.; Memon, J.; Wang, C.; Geng, J.; Huang, Y. Scalable Preparation of Three-Dimensional Porous Structures of Reduced Graphene Oxide/Cellulose Composites and Their Application in Supercapacitors. *Carbon* **2013**, *62*, 501−509.

(21) Stoller, M. D.; Park, S.; Zhu, Y.; An, J.; Ruoff, R. S. Graphene-Based Ultracapacitors. *Nano Lett.* **2008**, *8*, 3498−3502.

(22) Zhang, C.; Xie, Y.; Zhao, A.; Pentecost, A. E.; Ling, Z.; Wang, J.; Long, D.; Ling, L.; Qiao, W. Enhanced Electrochemical Performance of Hydrous RuO_2/Mesoporous Carbon Nanocomposites via Nitrogen Doping. *ACS Appl. Mater. Interfaces* **2014**, *6*, 9751−9759.

(23) Wang, W.; Guo, S.; Lee, I.; Ahmed, K.; Zhong, J.; Favors, Z.; Zaera, F.; Ozkan, M.; Ozkan, C. S. Hydrous Ruthenium Oxide Nanoparticles Anchored to Graphene and Carbon Nanotube Hybrid Foam for Supercapacitors. *Sci. Rep.* **2014**, DOI: 10.1038/srep04452.

(24) Subramanian, V.; Hall, S. C. P; Smith, P. H.; Rambabu, B. Mesoporous Anhydrous RuO_2 as a Supercapacitor Electrode Material. *Solid State Ionics* **2004**, *175*, 511−515.

(25) Yuan, Y. F.; Xia, X. H.; Wu, J. B.; Huang, X. H.; Pei, Y. B.; Yang, J. L.; Guo, S. Y. Hierarchically Porous Co_3O_4 Film with Mesoporous Walls Prepared via Liquid Crystalline Template for Supercapacitor Application. *Electrochem. Commun.* **2011**, *13*, 1123−1126.

(26) Zhu, T.; Chen, J. S.; Lou, X. W. Shape-Controlled Synthesis of Porous Co_3O_4 Nanostructures for Application in Supercapacitors. *J. Mater. Chem.* **2010**, *20*, 7015−7020.

DOI: 10.1021/acsami.5b02787
ACS Appl. Mater. Interfaces 2015, 7, 13503−13511

(27) Yang, D. Application of Nanocomopsites for Supercapacitors: Characteristics and Properties. In *Nanocomposites-New Trends and Developments;* Ebrahimi, F., Ed.; InTech: Rijeka, Croatia, 2012: Chapter 12, pp 299−328.
(28) He, G.; Li, J.; Chen, H.; Shi, J.; Sun, X.; Chen, S.; Wang, X. Hydrothermal Preparation of Co_3O_4@Graphene Nanocomposite for Supercapacitor with Enhanced Capacitive Performance. *Mater. Lett.* **2012**, *82*, 61−63.
(29) Xiang, C.; Li, M.; Zhi, M.; Manivannan, A.; Wu, N. A Reduced Graphene Oxide/Co_3O_4 Composite for Supercapacitor Electrode. *J. Power Sources* **2013**, *226*, 65−70.
(30) Shan, Y.; Gao, L. Formation and Characterization of Multi-Walled Carbon Nanotubes/Co_3O_4 Nanocomposites for Supercapacitors. *Mater. Chem. Phys.* **2007**, *103*, 206−210.
(31) Zhang, B.; Yu, Y.; Huang, Z. D.; He, Y. B.; Jang, D. H.; Yoon, W. S.; Mai, Y. W.; Kang, F. Y.; Kim, J. K. Exceptional Electrochemical Performance of Freestanding Electrospun Carbon Nanofiber Anodes Containing Ultrafine SnO_x Particles. *Energy Environ. Sci.* **2012**, *5*, 9895−9902.
(32) Zhang, B.; Xu, Z. L.; He, Y. B.; Abouali, S.; Akbari Garakani, M.; Kamali Heidari, E.; Kang, F.; Kim, J. K. Exceptional Rate Performance of Functionalized Carbon Nanofiber Anodes Containing Nanopores Created by (Fe) Sacrificial Catalyst. *Nano Energy* **2014**, *4*, 88−96.
(33) Zhang, B.; Xu, Z. L.; Abouali, S.; Akbari Garakani, M.; He, Y. B.; Kang, F.; Kim, J. K. Correlation Between Atomic Structure and Electrochemical Performance of Anodes Made from Electrospun Carbon Nanofiber Films. *Adv. Energy Mater.* **2014**, *4*, 1301448.
(34) Tai, Z.; Lang, J.; Yan, X.; Xue, Q. Mutually Enhanced Capacitances in Carbon Nanofiber/Cobalt Hydroxide Composite Paper for Supercapacitor. *J. Electrochem. Soc.* **2012**, *159* (4), A485−A491.
(35) Yang, W.; Gao, Z.; Ma, J.; Wang, J.; Wang, B.; Liu, L. Effects of Solvent on the Morphology of Nanostructured Co_3O_4 and Its Application for High-Performance Supercapacitors. *Electrochim. Acta* **2013**, *112*, 378−385.
(36) Abouali, S.; Akbari Garakani, M.; Zhang, B.; Luo, H.; Xu, Z. L.; Huang, J. Q.; Huang, J.; Kim, J. K. Co_3O_4/Porous Electrospun Carbon Nanofibers as Anodes for High Performance Li-Ion Batteries. *J. Mater. Chem. A* **2014**, *2*, 16939−16944.
(37) Ryu, W. H.; Shin, J.; Jung, J. W.; Kim, I. D. Cobalt(II) Monoxide Nanoparticles Embedded in Porous Carbon Nanofibers as a Highly Reversible Conversion Reaction Anode for Li-Ion Batteries. *J. Mater. Chem. A* **2013**, *1*, 3239−3243.
(38) Dìaz, J.; Paolicelli, G.; Ferrer, S.; Comin, F. Separation of the sp^3 and sp^2 Components in the C1*s* Photoemission Spectra of Amorphous Carbon Films. *Phys. Rev. B* **1996**, *54* (11), 8064−8069.
(39) Petitto, S. C.; Marsh, E. M.; Carson, G. A.; Langell, M. Cobalt Oxide Surface Chemistry: The Interaction of CoO (100), Co_3O_4 (110), and Co_3O_4 (111) with Oxygen and Water. *J. Mol. Catal. A: Chem.* **2008**, *281*, 49−58.
(40) Cong, H. P.; Yu, S. H. Shape Control of Cobalt Carbonate Particles by a Hydrothermal Process in a Mixed Solvent: An Efficient Precursor to Nanoporous Cobalt Oxide Architectures and Their Sensing Property. *Cryst. Growth Des.* **2009**, *9* (1), 210−217.
(41) Li, B.; Xie, Y.; Wu, C.; Li, Z.; Zhang, J. Selective Synthesis of Cobalt Hydroxide Carbonate 3D Architectures and Their Thermal Conversion to Cobalt Spinel 3D Superstructures. *Mater. Chem. Phys.* **2006**, *99*, 479−486.
(42) Zielke, U.; Huttinger, K. J.; Hoffman, W. P. Surface-Oxidized Carbon Fibers: I. Surface Structure and Chemistry. *Carbon* **1996**, *34*, 983−998.
(43) Barakat, N. A. M.; Kim, B.; Park, S. J.; Jo, Y.; Jung, M. H.; Kim, H. Y. Cobalt Nanofibers Encapsulated in a Graphite Shell by an Electrospinning Process. *J. Mater. Chem.* **2009**, *19*, 7371−7378.
(44) Zhang, B.; Xu, Z. L.; Kim, J. K. In Situ Grown Graphitic Carbon/Fe_2O_3/Carbon Nanofiber Composites for High Performance Freestanding Anodes in Li-Ion Batteries. *RSC Adv.* **2014**, *4*, 12298−12301.
(45) Ōya, A.; Ōtani, S. Catalytic Graphitization of Carbons by Various Metals. *Carbon* **1979**, *17*, 131−137.
(46) Ōya, A. Review: Phenomena of Catalytic Graphitization. *J. Mater. Sci.* **1982**, *17*, 309−322.
(47) Sevilla, M.; Fuertes, A. B. Catalytic Graphitization of Templated Mesoporous Carbons. *Carbon* **2006**, *44*, 468−474.
(48) Xu, Z. L.; Zhang, B.; Abouali, S.; Akbari Garakani, M.; Huang, J.; Huang, J. Q.; Heidari, E. K.; Kim, J. K. Nanocavity-Engineered Si/Multi-Functional Carbon Nanofiber Composite Anodes with Exceptional High-Rate Capacities. *J. Mater. Chem. A* **2014**, *2*, 17944−17951.
(49) Chu, P. K.; Li, L. Characterization of Amorphous and Nanocrystalline Carbon Films. *Mater. Chem. Phys.* **2006**, *96*, 253−277.
(50) Jerng, S. K.; Yu, D. S.; Lee, J. H.; Kim, C.; Yoon, S.; Chun, S. H. Graphitic Carbon Growth on Crystalline and Amorphous Oxide Substrates Using Molecular Beam Epitaxy. *Nanoscale Res. Lett.* **2011**, *6*, 565−570.
(51) Xie, F. Y.; Xie, W. G.; Gong, L.; Zhang, W. H.; Chen, S. H.; Zhang, Q. Z.; Chen, J. Surface Characterization on Graphitization of Nanodiamond Powder Annealed in Nitrogen Ambient. *Surf. Interface Anal.* **2010**, *42*, 1514−1518.
(52) Popov, C.; Kulisch, W.; Boycheva, S.; Yamamoto, K.; Ceccone, G.; Kog, Y. Structural Investigation of Nanocrystalline Diamond/Amorphous Carbon Composite Films. *Diamond Relat. Mater.* **2004**, *13*, 2071−2075.
(53) Zhao, S.; Shi, Z. Q.; Wang, C. Y.; Chen, M. M. Structure and Surface Elemental State Analysis of Polyimide Resin Film after Carbonization and Graphitization. *J. Appl. Polym. Sci.* **2008**, *108*, 1852−1856.
(54) Takahagi, T.; Ishitani, A. XPS Study on the Surface Structure of Carbon Fibers Using Chemical Modification and C1s Line Shape Analysis. *Carbon* **1988**, *26* (3), 389−396.
(55) Xu, Z. L.; Zhang, B.; Zhou, Z. Q.; Abouali, S.; Akbari Garakani, M.; Huang, J. Q.; Huang, J. Q.; Kim, J. K. Carbon Nanofibers Containing Si Nanoparticles and Graphene-Covered Ni for High Performance Anodes in Li Ion Batteries. *RSC Adv.* **2014**, *4*, 22359−22366.
(56) Zhang, F.; Yuan, C.; Zhu, J.; Wang, J.; Zhang, X.; Lou, X. W. Flexible Films Derived from Electrospun Carbon Nanofibers Incorporated with Co_3O_4 Hollow Nanoparticles as Self-Supported Electrodes for Electrochemical Capacitors. *Adv. Funct. Mater.* **2013**, *23*, 3909−3915.
(57) Xia, X.; Tu, J.; Zhang, Y.; Mai, Y.; Wang, X.; Gu, C.; Zhao, X. Freestanding Co_3O_4 Nanowire Array for High Performance Supercapacitors. *RSC Adv.* **2012**, *2*, 1835−1841.
(58) Guan, Q.; Cheng, J.; Wang, B.; Ni, W.; Gu, G.; Li, X.; Huang, L.; Yang, G.; Nie, F. Needle-Like Co_3O_4 Anchored on the Graphene with Enhanced Electrochemical Performance for Aqueous Supercapacitors. *ACS Appl. Mater. Interfaces* **2014**, *6*, 7626−7632.
(59) Tummala, R.; Guduru, R. K.; Mohanty, P. S. Nanostructured Co_3O_4 Electrodes for Supercapacitor Applications from Plasma Spray Technique. *J. Power Sources* **2012**, *209*, 44−51.

DOI: 10.1021/acsami.5b02787
ACS Appl. Mater. Interfaces 2015, 7, 13503−13511